Optics Letters

In-vivo retinal imaging with off-axis full-field time-domain optical coherence tomography

Helge Sudkamp,[1,2,*] Peter Koch,[1] Hendrik Spahr,[1,2] Dierck Hillmann,[3] Gesa Franke,[1,2] Michael Münst,[1] Fred Reinholz,[1,2] Reginald Birngruber,[1,2] and Gereon Hüttmann[1,2,4]

[1]Medical Laser Center Lübeck GmbH, Peter-Monnik-Weg 4, 23562 Lübeck, Germany
[2]Institute of Biomedical Optics, University of Lübeck, Peter-Monnik-Weg 4, 23562 Lübeck, Germany
[3]Thorlabs GmbH, Maria-Goeppert-Straße 9, 23562 Lübeck, Germany
[4]Airway Research Center North (ARCN), Member of the German Center for Lung Research (DZL), 35392 Gießen, Germany
*Corresponding author: sudkamp@mll.uni-luebeck.de

Received 1 September 2016; revised 28 September 2016; accepted 28 September 2016; posted 29 September 2016 (Doc. ID 274656); published 25 October 2016

With a simple setup, mainly composed of a low coherence light source and a camera, full-field optical coherence tomography (FF-OCT) allows volumetric tissue imaging. However, fringe washout constrains its use in retinal imaging. Here, we present a novel motion-insensitive approach to FF-OCT, which introduces path-length differences between the reference and the sample light in neighboring pixels using an off-axis reference beam. The temporal carrier frequency in scanned time-domain OCT is replaced by a spatial carrier frequency. Volumetric *in-vivo* FF-OCT measurements of the human retina were acquired in only 1.3 s, comparable to the acquisition times of current clinically used OCT devices.

OCIS codes: (110.0110) Imaging systems; (110.1650) Coherence imaging; (110.4500) Optical coherence tomography; (110.3175) Interferometric imaging; (070.2615) Frequency filtering; (170.4500) Optical coherence tomography.

http://dx.doi.org/10.1364/OL.41.004987

Optical coherence tomography (OCT) uses polychromatic light interference to obtain depth-resolved backscattering profiles (A-scans) of biological tissues. The focused beam scans across the tissue, acquiring cross-sectional tomographic images.

Interference detection in OCT is inherently phase sensitive. Within the acquisition time, relative motions of a few hundred nanometers between the sample and reference reduce the interference contrast (a phenomenon known as fringe washout). Hence, involuntary eye movements of the patient limit the maximum acquisition time of an interferogram from 200 μs to 1 ms, depending on the required image quality and clinical setting [1,2].

Historically, fringe washout needed to be overcome before bringing OCT technologies into the clinical environment. Time-domain OCT (TD-OCT) in ophthalmology was adopted only after the development of fast phase modulators. Similarly, Fourier-domain OCT (FD-OCT) improves the sensitivity of OCT via axial parallelization, but was not utilized in retinal imaging until line cameras with kHz line rates became available. Retinal imaging with full-field swept-source OCT systems (FF-SS-OCT) [3,4], which combines a tunable laser and a 2D camera without beam scanning, became possible when ultrafast cameras with a 100 kHz regime frame rate were developed [3]. At such extreme measurement speeds, the entire volume (instead of a single A-scan) can be imaged within the fringe washout limit.

As the number of detected photons determines the signal-to-noise ratio (SNR), the maximum permissible exposure (MPE) directly limits the acquisition rate and sensitivity of OCT. In scanning clinical OCT devices, the focused illumination sets the applicable power to approximately 1 mW, depending on the central wavelength used. Full-field OCT (FF-OCT) uses extended illumination, increasing the OCT throughput by more than an order of magnitude. In a simple optical setup with no lateral scanners, the interference pattern at multiple lateral positions is directly detected by a 2D camera.

Full-field time-domain OCT (FF-TD-OCT) acquires an en-face image in different depths in the tissue by adapting the path length of the reference arm. To reconstruct the OCT signal at each depth position, a set of at least two phase-shifted measurements must be taken within 1 ms. Retinal imaging by this process requires minimum frame rates of 2–10 kHz. Therefore, *in-vivo* imaging of FF-TD-OCT was demonstrated only in the anterior segment of an anesthetized rat [5], but has not been attempted in humans. The readout rate of the camera can be reduced by single-shot imaging of the interference pattern at different phases. However, previous approaches [6,7] are too complicated for *in-vivo* imaging.

To simplify the FF-TD-OCT imaging process, we present a novel motion-insensitive approach using an off-axis reference beam [8,9], which introduces path-length differences between the reference and the sample light in neighboring pixels. While an off-axis reference was previously used in short coherence holography [10] and in electronic speckle pattern interferometry for surface metrology with coherent light sources [11], it

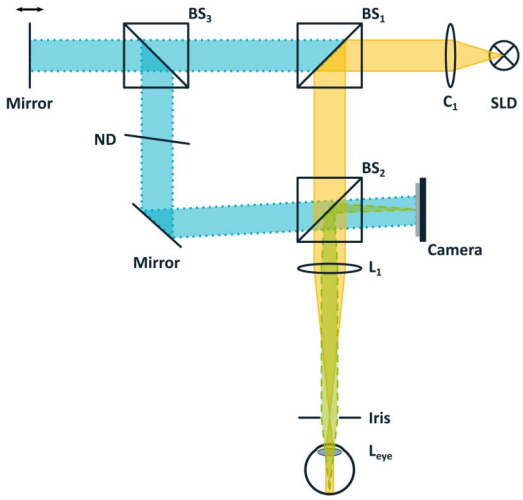

Fig. 1. Setup of off-axis full-field time-domain OCT: C_1 is the collimating lens; BS_1, BS_2, and BS_3 are beam splitters; L_1 is an achromatic lens; L_{eye} are the refractive elements of the eye; and ND is a neutral density filter. The diaphragm iris is placed in the Fourier plane of both lenses.

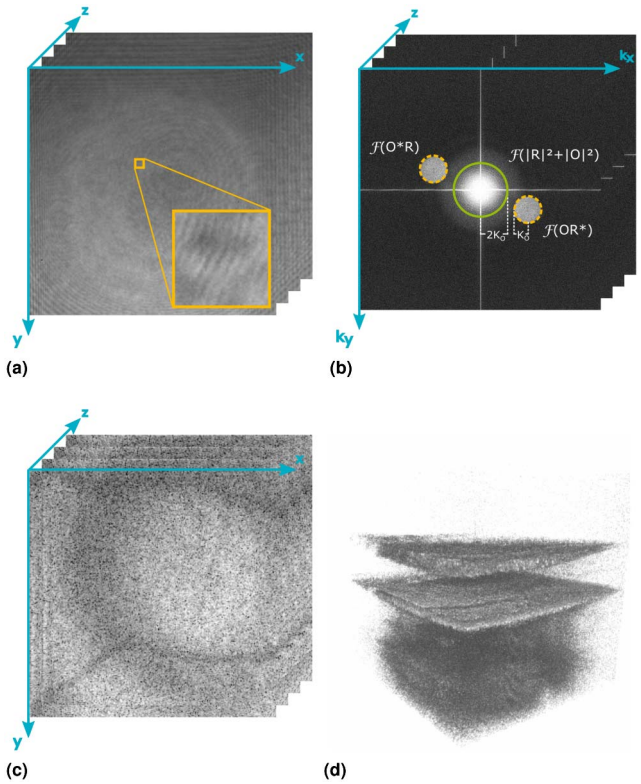

Fig. 2. Image reconstruction steps: (a) image of a human retina superimposed with the reference light. The inset shows a (50 × 50)-pixel area with an enhanced contrast. Speckling from the sample and fringe pattern caused by interference with the reference wave is clearly visible. (b) Fourier transformed image. Orange (dotted) and green (solid) circles indicate the cross-correlation and autocorrelation terms, respectively. (c) En-face image after inverse Fourier transform of a cross-correlation term in log-scale. (d) 3D rendering of the volume in log-scale.

was never used for volumetric *in-vivo* imaging. We use this approach to acquire single-shot en-face images *in-vivo* and, by step-wise changing the reference arm length between acquisitions, reconstruct volumetric images of human retina.

Although the proposed method is applicable to general *in-vivo* imaging, we report only on retinal imaging as a benchmark for OCT imaging. The setup in Fig. 1 was designed for this specific application.

The spatially coherent light source is a 36 mW superluminescent diode (BroadLighter M-S-840-G-I-30, Superlum) with a central wavelength of $\lambda_0 = 841$ nm and a spectral bandwidth of $\Delta\lambda = 23.6$ nm. As the spectral profile is nearly Gaussian, the expected axial resolution is 13 µm full width at half-maximum in air. The light is collimated by lens C_1 to a beam diameter of 16.6 mm ($1/e^2$ intensity decrease).

The open interferometer divides light into a reference arm (blue, dotted) and sample arm (yellow, solid) by a 90:10 beam splitter (BS_1). The light in the sample arm passes through a second beam splitter (BS_2) and is focused by an achromatic lens L_1 (focal length = 125 mm) onto the front focal point of the human eye. The eye optics further collimate the light into a parallel beam on the retina. The combined imaging by lens L_1 and the eye ($f = 16.6$ mm) yields a magnification M of 7.5 and an illumination beam diameter of 2.2 mm on the retina. Each point of the retina is then imaged by the ocular system and L_1 onto a camera (acA2040 180 km NIR, Basler) with a pixel spacing and active area of 5.5 µm and 2040 × 2048 pixel, respectively. The quantum efficiency at 830 nm is 35% with a full well capacity (FWC) of 13,500 electrons.

The field of view (FOV) is limited by the dimensions of the camera chip (11.2 × 11.2 mm) and the magnification M to approximately 1.5 × 1.5 mm. An iris of the diameter 2 mm is placed at the common Fourier plane of the eye optics (L_{eye}) and L_1, corresponding to a chosen numerical aperture of 0.06.

In the reference arm, light is reflected by a mirror mounted on a linear stage. During each volume measurement, the reference mirror is moved once through the axial measurement range. The reference light is directed onto the camera at an off-axis angle of 1.5°.

The intensity pattern on the camera [Fig. 2(a)], created by interference between object (O) and reference (R) radiation, can be decomposed into four parts:

$$I = |R + O|^2 = |R|^2 + |O|^2 + RO^* + R^*O. \quad (1)$$

As occurs in digital holography [12], the off-axis reference beam introduces a spatial carrier frequency to the interference pattern I on the camera. This frequency corresponds to the temporal carrier frequency in scanning TD-OCT. In the Fourier domain, the off-axis reference shifts both cross-correlation terms, which result from interference between the object (O) and reference (R) radiations (R^*O and RO^*), away from the autocorrelation terms $|R|^2$ and $|O|^2$. At some suitable angle between the object and the reference light, the cross-correlation and autocorrelation terms are completely separated. The bandwidth K_O of the spatial frequencies of the object signal depends on the numerical aperture NA of the setup and the wavelength λ_0 as follows:

$$K_O = \frac{2 \cdot \pi \cdot \mathrm{NA}}{\lambda_0}. \quad (2)$$

Self-interference doubles the bandwidth of the autocorrelation term $|O|^2$. To separate the signal terms $R^* O$ and RO^* from the autocorrelation terms, the signal terms must be shifted from the zero frequency by at least $3K_O$. To achieve this separation in a setup with a circular aperture and a square detector, each spatial frequency of the signal needs to be sampled by at least 13 pixels [13]. The lateral oversampling increases the overheads of the image sensor readout and subsequent signal processing. However, this approach also bins the pixels, increasing the effective full well capacity of each reconstructed voxel and, consequently, SNR and the dynamic range of the signal.

The OCT signals were demodulated by a 2D Fourier transform of the frames [Fig. 2(b)]. One cross-correlation term was selected by a bandpass filter; all other frequencies were suppressed. The selected cross-correlation term was then centered on the zero frequency, which corresponds to shifting the signal term into the baseband and removal of the carrier frequency. Inverse Fourier transformation yielded the en-face image shown in Fig. 2(c), which was slightly tilted by the off-axis angle of 1.5°. By moving the reference mirror, we obtained a set of en-face scans at different depths, which can be assembled into a complete volume [Fig. 2(d)].

The sensitivity Σ_{dB} of a shot-noise-limited OCT system is fundamentally limited by the number of electrons ($N_{\mathrm{e,voxel}}$) collected for each voxel of the sample [14]. In off-axis full-field OCT, the amplitude of an interference signal is also proportional to the modulation transfer function (MTF) of the image sensor [15]. The crosstalk between the pixels reduces the modulation contrast and, thus, the OCT signal in a frequency-dependent manner. Therefore, the sensitivity is proportional to the square of the MTF at the spatial carrier frequency chosen for the setup:

$$\Sigma_{\mathrm{dB}} = 20 \log\left(\mathrm{MTF} \cdot \sqrt{N_{\mathrm{e,voxel}}}\right), \tag{3}$$

with

$$N_{\mathrm{e},v\mathrm{oxel}} = \frac{\Phi \cdot \mathrm{QE} \cdot t_{\mathrm{exp}} \cdot T \cdot \lambda_0}{N_{\mathrm{voxel}} \cdot c \cdot h}. \tag{4}$$

In this equation, c is the speed of light, and h is Planck's constant. Note that the sensitivity can be increased by increasing the center wavelength λ_0 of the light source, the quantum efficiency QE of the camera, the transmission T between the sample and camera, the incident radiant flux Φ in the imaged FOV, and the exposure time t_{exp}. After filtering in the Fourier domain, the number of voxels N_{voxel} in the final image depends on the optical sampling set by the imaging optics. Conversely, the sensitivity decreases by increasing N_{voxel} (i.e., refining the sampling of the object) and by the pixel crosstalk of the camera, which causes losses in the modulation transfer function. Two of the above sensitivity-enhancing factors are crucially constrained in retinal imaging:

(1) The maximum radiant flux on the retina is restricted by laser safety regulations. The maximum permissible flux in scanning OCT is approximately 800 μW. In full-field OCT, the maximum permissible flux increases to approximately 50 mW under a 2 mm illuminated field.

(2) The second constraint on the sensitivity is imposed by the maximum exposure time, which is limited by the fringe washout time. In our FF-OCT, an exposure time of 400 μs sufficiently compromises between the motion sensitivity and the number of detected photons.

The system layout required a trade-off between the sensitivity and the number of voxels in one en-face image. At a desired sensitivity of 80 dB and the light source-limited maximum radiant flux of 11 mW into the eye, the number of independent voxels is limited by Eqs. (3) and (4) to only 47,000.

In scanning OCT systems, the distance between the sampling points is independent of the lateral resolution. Sparse sampling is often chosen in one or both axes for volume scans but, in FF-OCT, dense sampling along both lateral dimensions is intrinsic. Therefore, given our camera and the chosen NA, the maximum lateral (FOV) was 1.7 mm × 1.7 mm with a lateral voxel size of 6.9 μm.

In our setup, we used a commercially available lens L_1 with $f = 125$ mm, which reduced the actual FOV to 1.5 mm × 1.5 mm. The aperture was adjusted to yield the 47,000 voxels in the OCT image, which guarantees the quantum noise-limited sensitivity of 80 dB. Thus, each independent voxel, i.e., each speckle, is sampled by 87 pixels (2040 × 2048 pixel, 47,000 voxels) of the camera. Accumulation of the FWC from all pixels within one voxel provides three orders of magnitude or a 60 dB dynamic range of the measurement.

Because the intensity profile of the illuminating beam is Gaussian, the sensitivity in the voxels is higher in the center of the en-face image than at the edges. In calculations of the beam profile, the sensitivity was determined as 82 dB in the center, dropping to 74 dB at the edges.

Although our carrier frequency was 0.17 pixel^{-1} and, thus, approximately 0.34 times the Nyquist limit, the maximum interference contrast was only 65% (confirmed by independent measurements of the camera MTF). Hence, the central sensitivity should drop by 3.7–78.3 dB. By placing a gold mirror behind a calibrated neutral density filter (with OD = 3.2) and carefully compensating for the mismatched group velocity dispersion between the sample and the reference arms, we measured the central sensitivity as 77 dB.

The axial resolution was measured as 12 μm in air; correspondingly, the retinal structures were resolved to approximately 9 μm.

A human retina was imaged with our TD-FF-OCT in healthy subjects (Fig. 3). With a 187 Hz camera frame rate, each retinal volume (238 × 238 effective lateral voxels and 250 depth slices corresponding to 1.5 mm × 1.5 mm × 1.4 mm FOV) was acquired within 1.3 s, corresponding to an effective A-scan rate of 43 kHz. Multiple retinal layers in the macula are clearly visible [Figs. 3(a) and 3(b)]. More peripheral areas were also imaged with good quality [Fig. 3(c)]. Eye motions caused a loss of interference contrast and appeared as horizontal lines of low or no signal in the B-scan [Fig. 3(d)].

In contrast to FD-OCT, TD-OCT detects scattered light from a single depth, which reduces its sensitivity by approximately 30 dB (relative to FD-OCT) and limits the A-scan rate of clinical TD-OCT devices to a few kHz. Here, we achieved surprisingly good image quality at an effective A-scan rate of 43 kHz and a radiant flux increase of only 14 times (relative to TD-OCT).

This subjectively high image quality probably results from the high photon collection efficiency of wide-field imaging. Scanning OCT devices suppress light in the outer parts of the point spread function by confocal gating, improving the

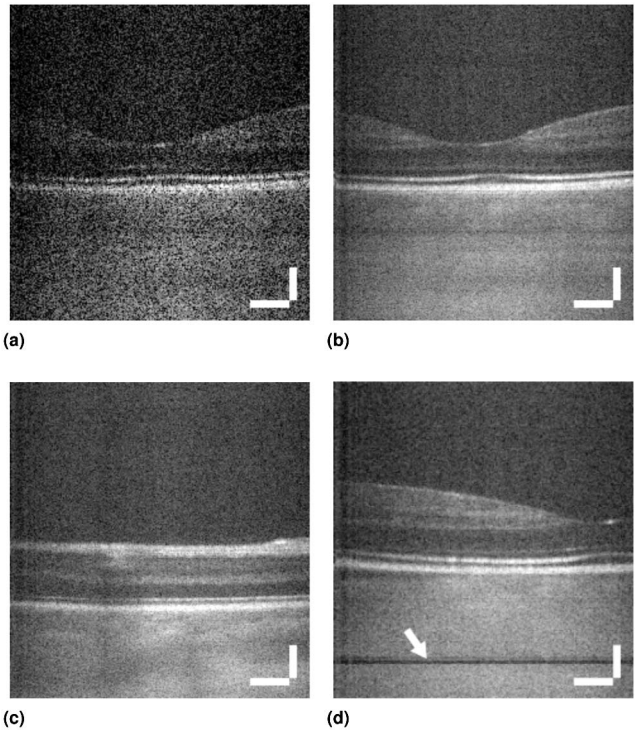

Fig. 3. Retinal images of a healthy eye captured *in-vivo*. Shown are B-scans of (a) the *macula* region; (b) the *macula* region, averaged among 10 lateral frames; (c) the peripheral region, averaged among 10 lateral frames; and (d) a *macula* with severe motion artifacts (arrow), averaged among 10 lateral frames. The scale bars are 200 μm.

resolution at the cost of reduced sensitivity. With its spatially coherent illumination, FF-TD-OCT detects photons that have been slightly diverted by the eye optics at neighboring lateral positions. Therefore, these pixels contribute to the detected signal and increase the SNR in tissues with relatively few lateral structures, but prominent axial structures.

As FF-TD-OCT with coherent illumination accepts multiple scattered photons, all retinal images show strong featureless signals below the retinal pigment epithelium (RPE), where the light scattering is high. Moreover, because multiple scattering increases the propagation length in the tissue, these photons are assigned to false axial locations at depths below the RPE. The multiple scattered photons could be suppressed by using a spatially incoherent light source which, however requires a highly symmetric interferometer and, thus, is not easily applicable to our off-axis approach [16].

Both of the above effects are also recognized in FF-SS-OCT, which offers a similar image quality [3,4,17]. With FF-SS-OCT, the image quality was sufficiently high to even visualize single photoreceptor cells when numerical aberration correction was used [18].

The integration time of each frame in our FF-TD-OCT system is 400 μs, one order of magnitude longer than that in current clinical FD-OCT devices. To date, the longest reported integration time in a clinical OCT device is 200 μs [1]. Nevertheless, although motion artifacts were rarely visible with healthy subjects, our acquisition times must be shortened before employing our system in a clinical setting to cater for patients with fixation difficulties. An increase of imaging speed without sacrificing sensitivity is possible by increasing the radiant flux or decreasing the FOV.

In summary, we have shown a novel approach for parallelized TD-OCT. The phase and amplitude information of a complete en-face OCT image can be measured within a single exposure time of a few hundred microsecond and with a depth resolution of 9 μm in biological tissue. Volumetric OCT images are reconstructed by changing the length of the reference arm. Due to the parallel acquisition of the lateral information, the human retina was imaged *in-vivo* at an effective A-scan rate of 43 kHz. The quality was sufficiently high to discriminate relevant tissue layers. The inherently lower sensitivity of TD-OCT compared to that of FD-OCT was partially compensated by the higher MPE and more efficient detection of scattered light in the full-field imaging geometry.

Funding. Bundesministerium für Bildung und Forschung (BMBF) (13N13763).

REFERENCES

1. M. Stehouwer, F. D. Verbraak, H. R. de Vries, and T. G. van Leeuwen, Eye **25**, 97 (2011).
2. M. Mueller, C. Schulz-Wackerbarth, P. Steven, E. Lankenau, T. Bonin, H. Mueller, A. Brueggemann, R. Birngruber, S. Grisanti, and G. Huettmann, Curr. Eye Res. **35**, 722 (2010).
3. T. Bonin, G. Franke, M. Hagen-Eggert, P. Koch, and G. Hüttmann, Opt. Lett. **35**, 3432 (2010).
4. H. Spahr, D. Hillmann, C. Hain, C. Pfäffle, H. Sudkamp, G. Franke, and G. Hüttmann, Opt. Lett. **40**, 4771 (2015).
5. K. Grieve, A. Dubois, M. Simonutti, M. Paques, J. Sahel, J.-F. Le Gargasson, and C. Boccara, Opt. Express **13**, 6286 (2005).
6. M. Akiba, K. P. Chan, and N. Tanno, Opt. Lett. **28**, 816 (2003).
7. C. Dunsby, Y. Gu, and P. French, Opt. Express **11**, 105 (2003).
8. E. Leith and J. Upatnieks, J. Opt. Soc. Am. **52**, 1123 (1962).
9. D. Hillmann, G. Franke, L. Hinkel, T. Bonin, P. Koch, and G. Hüttmann, Proc. SPIE **8571**, 857104 (2013).
10. S. Witte, A. Plauşka, M. C. Ridder, L. van Berge, H. D. Mansvelder, and M. L. Groot, Biomed. Opt. Express **3**, 2184 (2012).
11. M. Takeda, H. Ina, and S. Kobayashi, J. Opt. Soc. Am. **72**, 156 (1982).
12. E. Cuche, P. Marquet, and C. Depeursinge, Appl. Opt. **39**, 4070 (2000).
13. D. Hillmann, *Holoscopy* (Springer, 2014).
14. E. A. Swanson, D. Huang, M. R. Hee, J. G. Fujimoto, C. P. Lin, and C. A. Puliafito, Opt. Lett. **17**, 151 (1992).
15. P. Koch, G. Hüttmann, H. Schleiermacher, and E. Koch, Opt. Lett. **29**, 1644 (2004).
16. A. Dubois, L. Vabre, A.-C. Boccara, and E. Beaurepaire, Appl. Opt. **41**, 805 (2002).
17. D. Hillmann, C. Lührs, T. Bonin, P. Koch, and G. Hüttmann, Opt. Lett. **36**, 2390 (2011).
18. D. Hillmann, H. Spahr, C. Hain, H. Sudkamp, G. Franke, C. Pfäffle, C. Winter, and G. Hüttmann, Sci. Rep. (2016).